

## Tivanite, a new oxyhydroxide mineral from Western Australia, and its structural relationship to rutile and diaspore

IAN E. GREY

CSIRO Division of Mineral Chemistry  
P.O. Box 124, Port Melbourne, Victoria 3207, Australia

AND ERNEST H. NICKEL

CSIRO Division of Mineralogy  
Wembley, W.A. 6014, Australia

### Abstract

Tivanite,  $V_{4.37}Fe_{0.14}Ti_{3.49}O_{11.49}(OH)_{4.51}$  (ideal  $VTiO_3OH$ ), is a new mineral species that has been found in the "green leader" gold lodes at Kalgoorlie, Western Australia. It is monoclinic with space group  $P2_1/c$ ,  $a = 7.494(5)$ ,  $b = 4.552(4)$ ,  $c = 10.005(8)\text{\AA}$ ,  $\beta = 129.79(2)^\circ$ ,  $Z = 1$ . The strongest powder diffraction lines (calculated) are  $3.880(100)(11\bar{1})$ ,  $2.795(94)(21\bar{1})$ ,  $2.636(69)(11\bar{3})$ ,  $1.683(31)(22\bar{4})$ ,  $1.693(30)(122)$ ,  $3.917(25)(011)$ .

Tivanite occurs as minute multiply twinned crystals in quartz. Associated minerals are vanadian muscovite and nolanite. Tivanite is black with a submetallic luster, lacks internal reflections, is moderately anisotropic, and has a specific gravity of 4.17 (calc.). Reflectivity values are 470 nm 16.8%, 546 nm 17.4%, 589 nm 17.7%. The microhardness is VHN 650 under a 50 g load.

The structure has been determined and refined to  $R = 0.12$  using intensities collected for a multiply twinned crystal by the Weissenberg technique, using  $CuK\alpha$  radiation. The structure is based on an ordered occupation by  $V^{3+}$  and  $Ti^{4+}$  of half of the octahedral sites in a hexagonal closest-packed anion array. It can be described as an ordered 1:1 intergrowth of  $TiO_2$  with a rutile-type structure and  $VOOH$  with a diaspore-type structure.

### Introduction

Concentrations of bright green material in the "Golden Mile" of Kalgoorlie, which carry particularly high gold values, are known locally as "green leader" and consist mainly of quartz, sericitic muscovite, carbonates, and pyrite. A recent investigation of "green leader" samples (Nickel, 1977) showed that the assemblage is rich in vanadium minerals. These include vanadium-bearing sericitic muscovite, which is responsible for the green color of the deposit, nolanite, tomichite (Nickel and Grey, 1979), and a new titanium-rich vanadium oxyhydroxide that is optically indistinguishable from nolanite but that has a quite different, previously unreported, X-ray diffraction pattern. The mineral is named tivanite, from the two main metal constituents. The mineral name and designation as a new mineral were approved by the Commission on New Minerals and Mineral Names of the International Mineralogical Association in

July 1980. A type specimen is in the collection of the CSIRO Division of Mineralogy, Floreat Park, Western Australia.

### Occurrence

The existence of tivanite was first mentioned by Nickel (1977), who referred to it as a titanium vanadate. Only one grain of it was recognized at that time and no additional material has been found since, in spite of intensive searching. The grain, which is in a polished section, measures about  $300 \times 90 \mu\text{m}$ , has an irregular outline, and contains numerous minute quartz inclusions and veins. The grain consists of many small irregular crystallites ( $5\text{--}30 \mu\text{m}$ ) occurring in twin relationships (various crystallites extinguish simultaneously between crossed nicols). The associated minerals are quartz, vanadium-bearing muscovite, and nolanite. The sample comes

from the Lake View mine, Kalgoorlie, Western Australia.

### Chemistry

The composition of tivanite has been determined from electron microprobe analyses combined with a crystal structure determination. The average of three microprobe analyses, using metal standards for all elements, gives  $V_2O_3$  48.27%,  $TiO_2$  41.03%,  $Fe_2O_3$  1.57%,  $H_2O$  (calc.) 5.97%, total 96.84%. No other elements with an atomic number of more than 11 were found. The low summation may be due partly to errors in estimating the effect of overlapping  $TiK\beta$  and  $VK\alpha$  peaks, and partly to the use of metal rather than oxide standards. The assignment of all vanadium as trivalent is consistent with the proposed valency state of vanadium in the associated vanadian muscovite (Nickel, 1977).

The crystal structure analysis, given below, established a hexagonal closest-packed anion arrangement, with sixteen anions per unit cell, and an anion-to-cation ratio of 2. Combined with the results of the microprobe analyses, this gives a unit-cell composition of  $V_{4.37}^{3+}Fe_{0.14}^{3+}Ti_{3.49}O_{11.49}(OH)_{4.51}$ . Grouping the vanadium and iron and rounding to one decimal gives a composition of  $V_{4.5}Ti_{3.5}O_{11.5}OH_{4.5}$ , *i.e.*, a composition that lies on the line between  $VOOH$  and  $TiO_2$ ,  $(VOOH)_{4.5}(TiO_2)_{3.5}$ , close to the 1:1 composition  $VTiO_3OH$ .

### Physical and optical properties

Tivanite is black with a black streak and a metallic to submetallic luster. It is opaque to light and does not exhibit internal reflections in either air or oil. In polished section, the reflection color is gray in air and pinkish gray in oil. Tivanite's reflection color in air is indistinguishable from that of nolanite, whereas in oil it is slightly less pink than nolanite. Reflection pleochroism is indiscernible. Anisotropism between crossed polars is weak to moderate, with various shades of gray. Average reflectances measured in air are 470 nm 16.8%, 546 nm 17.4%, 589 nm 17.7%.

The Vickers microhardness under a 50 g load is  $650 \pm 100$  kg/mm<sup>2</sup>. Because of the small size of the grain and the presence of quartz inclusions, the specific gravity could not be measured. The value calculated from X-ray data is 4.17.

### Crystallography

As discussed above, the sample grain of tivanite consists of clusters of irregular crystallites (5–30  $\mu$ m) in various twin relationships and separated from

each other by intrusive quartz veins. Attempts to isolate an individual crystallite were not successful. The specimen finally selected for study consisted of a dominant twin individual and four minor individuals (the volume of each minor individual was about 20% of the volume of the dominant individual). Precession photographs of this specimen displayed a pseudo-hexagonal array of strong reflections, corresponding to a subcell of  $a_h \approx 2.85 \text{ \AA}$ ,  $c_h \approx 4.55 \text{ \AA}$ , together with weaker, sharp superlattice reflections that could be indexed using a monoclinic cell with  $a_m = a_h + 3b_h$ ,  $b_m = c_h$ ,  $c_m = 2a_h - 2b_h$ . A powder diffraction pattern obtained from the main multiple-crystal grain of tivanite, using a 114.2 mm Debye-Scherrer camera, was indexed with this information. Refinement of the powder data gave the parameters for the monoclinic cell as  $a = 7.494(5)$ ,  $b = 4.552(4)$ ,  $c = 10.005(8) \text{ \AA}$ ,  $\beta = 129.79(2)^\circ$ . Because many of the powder pattern lines were overlain by lines stemming from the quartz inclusions, we could not obtain a complete observed pattern. Instead, we report, in Table 1, the pattern calculated from the structure refinement described below.

From the precession photographs, the systematic extinctions were  $(0k0)$ ,  $k = 2n + 1$ , and  $(h0l)$ ,  $l = 2n + 1$ , thus uniquely determining the space group as  $P2_1/c$ .

### Twinning

From the above unit-cell transformation, it can be shown that a pseudo-hexagonal superlattice of the monoclinic cell can be defined with  $a_s = 2a_m + 3c_m$ ,  $b_s = 2a_m - c_m$ ,  $c_s = b_m$ ,  $\beta = 120.14^\circ$  ( $a_s = b_s = 8a_m$ ). Twinning by reticular pseudomorph is expected,

Table 1. Tivanite: calculated powder diffraction pattern

$d$ (calc.)	$I/I_0$ (calc.)	$h k l$	$d$ (calc.)	$I/I_0$ (calc.)	$h k l$
5.758	4	1 0 0	2.001	1	3 1 $\bar{1}$
5.000	4	1 0 $\bar{2}$	1.940	1	2 2 $\bar{2}$
3.917	25	0 1 1	1.919	1	3 0 0
3.880	100	1 1 $\bar{1}$	1.855	1	4 0 $\bar{4}$
3.710	5	2 0 $\bar{2}$	1.814	1	2 0 2
2.837	13	1 1 $\bar{1}$	1.799	1	3 1 $\bar{3}$
2.795	94	2 1 $\bar{1}$	1.771	3	4 0 $\bar{2}$
2.636	69	1 1 $\bar{3}$	1.693	30	1 2 $\bar{2}$
2.602	3	2 1 $\bar{3}$	1.683	31	2 2 $\bar{4}$
2.535	24	1 0 2	1.674	1	1 1 $\bar{5}$
2.500	9	2 0 $\bar{4}$	1.670	24	3 2 $\bar{2}$
2.457	15	3 0 $\bar{2}$	1.666	1	3 0 $\bar{6}$
2.324	1	1 0 $\bar{4}$	1.632	18	4 1 $\bar{5}$
2.263	5	3 0 $\bar{4}$	1.616	3	2 0 $\bar{6}$
2.233	14	0 1 3	1.605	4	3 2 $\bar{4}$
2.214	23	1 1 2	1.586	1	4 0 $\bar{6}$
2.191	14	2 1 $\bar{4}$	1.537	10	3 1 1
2.173	1	3 1 $\bar{3}$	1.521	1	4 1 $\bar{1}$
2.162	21	3 1 $\bar{2}$	1.467	1	3 2 0
2.026	12	2 1 1	1.457	11	1 0 $\bar{6}$

with the twinning laws corresponding to the extra symmetry elements of the pseudohexagonal superlattice (Friedel, 1964). For the multiply twinned crystal studied with the precession method, the observed twinning laws are  $(102)_m$ ,  $(400)_m$ ,  $(30\bar{2})_m$ , and  $[010]_m^{60^\circ}$ , referred to the monoclinic cell. The twinning may equally well be considered to result from the pseudohexagonal symmetry of the subcell, which is due to the hexagonal closest-packed anion framework (see below). The twinning laws are those which leave the anion arrangement invariant. With reference to the subcell, the observed twinning laws are  $(100)_n$ ,  $(110)_n$ ,  $(010)_n$ , and  $[001]_n^{60^\circ}$ .

When the precession method was used with  $\text{MoK}\alpha$  radiation, the reflections from the various twin individuals at the monoclinic superlattice positions were all well separated, but those at the hexagonal subcell positions were just barely resolvable (Fig. 1). When the Weissenberg method was used with  $\text{CuK}\alpha$  radiation, the reflections from the twin individuals at the subcell nodes were also clearly resolved, and we decided to carry out a structure determination using intensities measured from Weissenberg photographs of the dominant twin individual.

#### Data collection and processing

For the collection of intensity data, the multiply twinned crystal described above, which measured  $50 \times 30 \times 20 \mu\text{m}$ , was aligned about the  $b$  axis. Intensity data for the levels  $h0l$  to  $h2l$  were obtained by the integrated Weissenberg technique, using nickel-filtered copper radiation and multiple film packs to increase the range of observations. The intensities were estimated visually using a calibrated film strip.

The reduction to structure factors and all subsequent computing was done on the CSIRO CDC-7600 computer, using the X-RAY 76 series of programs (Stewart, 1976). An absorption correction was applied ( $\mu = 577.2 \text{ cm}^{-1}$ ) on the assumption that the dominant twin individual had the same size and shape as the complete multiply twinned grain. Scattering curves for neutral metals and oxygen were taken from *International Tables for X-Ray Crystallography*, Vol. 2 (1962, p. 201ff). A composite scattering curve (0.45 Ti + 0.55 V) was used for the metals.

#### Structure solution and refinement

From the three-dimensional Patterson map the positions of two metal atoms were established. Refinement of the scale and the metal-atom coordinates for the 97 observed reflections reduced the conventional  $R$ -factor to 0.23. A Fourier map then revealed the

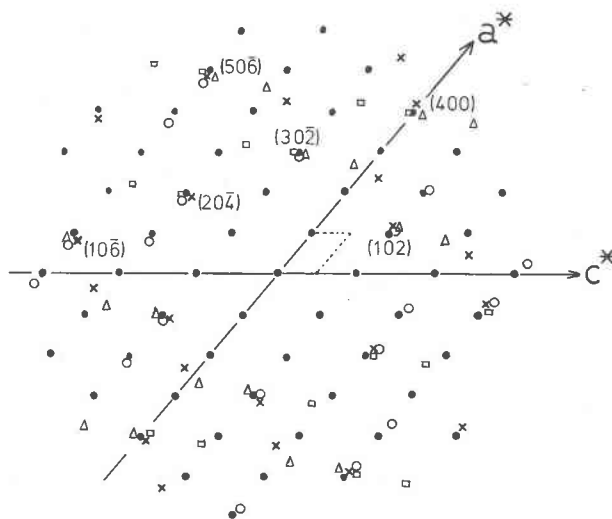


Fig. 1. Schematic representation of the  $(h0l)$  precession photograph obtained for a multiply twinned grain of tivanite. Reflections from the dominant twin individual are shown by the filled circles. Reflections due to twinning laws  $(400)_m$ ,  $(102)_m$ ,  $(30\bar{2})_m$ , and  $[010]_m^{60^\circ}$  are indicated by open circles, squares, crosses, and triangles respectively. The axes for the dominant twin individual are marked. For clarity, only the strong reflections from the four minor twin individuals are shown.

positions of four oxygen atoms. Inclusion of the oxygen atoms in the refinement, and subsequent refinement of all positional parameters and isotropic thermal parameters, resulted in an  $R$ -factor of 0.135 for all observed reflections. At this stage, the subcell reflections affected by twinning were removed, *i.e.*,  $(h00)_m$ ,  $(n02n)_m$ ,  $(3n0\bar{2}n)_m$ ,  $n = 1-3$ . Refinement of all parameters for the resulting 80 reflections gave a final  $R$ -factor of 0.12. The atomic coordinates and isotropic thermal parameters are given in Table 2. The large  $esd$ 's and high thermal parameters are the inevitable result of working with a multiply twinned crystal and not being able to make a satisfactory absorption correction. The general validity of the structure was confirmed by the agreement between the observed and calculated structure factors (Table 3) and by the bond lengths and angles associated with the

Table 2. Tivanite: final atomic coordinates and isotropic thermal parameters

Atom	$x$	$y$	$z$	$B(\text{\AA}^2)$
M(1)	0.105(1)	0.019(4)	0.183(1)	1.3(2)
M(2)	0.351(1)	0.019(4)	0.579(1)	2.6(2)
O(1)	0.134(4)	0.238(10)	0.355(3)	0.3(6)
O(2)	0.390(6)	0.239(14)	0.750(5)	3.4(10)
O(3)	0.636(5)	0.273(13)	0.107(4)	2.0(9)
O(4)	0.866(5)	0.263(13)	0.459(4)	1.9(8)

Table 3. Tivanite: observed and calculated structure factors

<i>h k l</i>	<i>F</i> (obs.)	<i>F</i> (calc.)	<i>h k l</i>	<i>F</i> (obs.)	<i>F</i> (calc.)	<i>h k l</i>	<i>F</i> (obs.)	<i>F</i> (calc.)	<i>h k l</i>	<i>F</i> (obs.)	<i>F</i> (calc.)
1 0 0	16.9	13.7	0 1 6	*	3.9	3 1 $\bar{6}$	*	9.9	3 2 4	*	13.8
1 0 2	112.3	80.4	0 1 7	16.8	12.4	3 1 $\bar{7}$	98.0	75.5	4 2 0	35.3	23.8
1 0 4	*	8.3	1 1 0	*	9.8	3 1 $\bar{8}$	*	2.1	4 2 1	*	3.7
1 0 6	11.5	14.9	1 1 1	34.0	40.8	3 1 $\bar{9}$	*	5.0	4 2 2	*	10.6
1 0 8	*	7.8	1 1 2	86.7	60.7	4 1 $\bar{1}$	33.2	21.7	4 2 3	*	3.1
2 0 0	8.7	8.5	1 1 3	*	10.2	4 1 $\bar{2}$	*	5.7	4 2 4	*	2.3
2 0 2	21.4	24.7	1 1 4	*	13.4	4 1 $\bar{3}$	*	9.6	5 2 0	28.9	26.6
2 0 4	49.5	53.4	1 1 5	27.9	37.0	4 1 $\bar{4}$	*	3.5	5 2 1	*	3.0
2 0 6	*	11.5	1 1 6	*	9.1	4 1 $\bar{5}$	87.7	93.1	5 2 2	31.8	41.8
3 0 0	28.0	16.7	1 1 7	29.2	36.4	4 1 $\bar{6}$	*	4.1	5 2 3	*	2.5
3 0 2	*	4.2	1 1 8	*	2.0	4 1 $\bar{7}$	*	7.5	1 2 $\bar{2}$	*	16.5
3 0 4	15.1	10.0	2 1 0	*	2.8	4 1 $\bar{8}$	37.3	32.8	1 2 $\bar{3}$	*	13.5
3 0 6	61.6	47.5	2 1 1	50.7	56.1	4 1 $\bar{9}$	*	11.0	1 2 $\bar{4}$	*	5.0
4 0 0	154.7	112.7	2 1 2	*	7.3	5 1 $\bar{1}$	*	9.6	1 2 $\bar{5}$	*	11.0
4 0 2	20.5	14.0	2 1 3	23.0	28.1	5 1 $\bar{2}$	*	4.6	1 2 $\bar{6}$	26.7	26.8
4 0 4	*	16.6	2 1 4	31.8	29.0	5 1 $\bar{3}$	74.4	73.5	2 2 $\bar{1}$	*	3.4
5 0 0	39.2	32.1	2 1 5	*	0.4	5 1 $\bar{4}$	*	2.9	2 2 $\bar{2}$	13.9	18.9
5 0 2	18.5	24.5	2 1 6	*	10.5	5 1 $\bar{5}$	*	8.8	2 2 $\bar{3}$	*	11.5
6 0 0	*	2.8	2 1 7	23.6	22.0	5 1 $\bar{6}$	*	1.6	2 2 $\bar{4}$	102.0	109.7
6 0 2	14.1	20.3	3 1 0	*	12.0	5 1 $\bar{7}$	*	5.4	2 2 $\bar{5}$	*	4.3
0 0 2	*	14.6	3 1 1	83.8	75.1	5 1 $\bar{8}$	*	7.2	2 2 $\bar{6}$	28.4	25.6
0 0 4	16.3	30.6	3 1 2	*	6.3	5 1 $\bar{9}$	*	2.4	3 2 $\bar{1}$	*	13.3
0 0 6	*	6.0	3 1 3	19.1	29.0	6 1 $\bar{1}$	46.7	48.2	3 2 $\bar{2}$	121.2	101.2
0 0 8	26.3	30.7	3 1 4	*	6.5	6 1 $\bar{2}$	*	6.7	3 2 $\bar{3}$	*	0.7
1 0 $\bar{2}$	13.6	18.2	3 1 5	15.4	17.6	6 1 $\bar{3}$	*	12.1	3 2 $\bar{4}$	41.0	53.1
1 0 $\bar{4}$	27.2	21.2	4 1 0	*	2.1	6 1 $\bar{4}$	25.5	18.0	3 2 $\bar{5}$	*	9.4
1 0 $\bar{6}$	97.9	112.8	4 1 1	*	1.9	6 1 $\bar{5}$	*	0.8	3 2 $\bar{6}$	21.8	17.3
2 0 $\bar{2}$	19.7	23.8	4 1 2	*	5.0	6 1 $\bar{6}$	*	8.1	4 2 $\bar{1}$	*	1.8
2 0 $\bar{4}$	66.5	65.0	4 1 3	35.8	38.5	6 1 $\bar{7}$	*	4.4	4 2 $\bar{2}$	33.5	40.1
2 0 $\bar{6}$	60.2	56.2	4 1 4	*	1.0	6 1 $\bar{8}$	*	3.7	4 2 $\bar{3}$	*	17.8
2 0 $\bar{8}$	19.7	13.1	4 1 5	*	16.4	6 1 $\bar{9}$	55.4	44.0	4 2 $\bar{4}$	*	13.0
3 0 $\bar{2}$	78.2	74.9	5 1 0	*	1.7	7 1 $\bar{1}$	*	10.0	4 2 $\bar{5}$	*	5.2
3 0 $\bar{4}$	51.8	46.2	5 1 1	20.3	15.6	7 1 $\bar{2}$	15.5	23.1	4 2 $\bar{6}$	*	11.1
3 0 $\bar{6}$	29.5	28.8	5 1 2	*	11.5	7 1 $\bar{3}$	*	5.9	4 2 $\bar{7}$	*	13.9
3 0 $\bar{8}$	*	2.7	5 1 3	*	5.3	7 1 $\bar{4}$	*	3.5	4 2 $\bar{8}$	53.3	41.0
4 0 $\bar{2}$	51.8	48.5	6 1 0	*	5.3	7 1 $\bar{5}$	*	7.4	5 2 $\bar{1}$	*	13.4
4 0 $\bar{4}$	21.2	20.7	6 1 1	*	4.5	7 1 $\bar{6}$	*	6.6	5 2 $\bar{2}$	*	9.4
4 0 $\bar{6}$	22.6	23.1	6 1 2	*	2.2	7 1 $\bar{7}$	45.9	46.6	5 2 $\bar{3}$	*	0.0
4 0 $\bar{8}$	42.0	28.5	1 1 $\bar{1}$	77.1	80.3	8 1 $\bar{2}$	*	0.5	5 2 $\bar{4}$	*	15.3
5 0 $\bar{2}$	*	1.7	1 1 $\bar{2}$	*	0.9	8 1 $\bar{3}$	*	6.5	5 2 $\bar{5}$	*	9.6
5 0 $\bar{4}$	19.5	26.6	1 1 $\bar{3}$	103.3	102.8	8 1 $\bar{4}$	*	3.8	5 2 $\bar{6}$	*	8.5
5 0 $\bar{6}$	92.3	86.8	1 1 $\bar{4}$	*	17.9	8 1 $\bar{5}$	35.1	35.6	5 2 $\bar{7}$	*	0.9
5 0 $\bar{8}$	61.5	57.6	1 1 $\bar{5}$	20.2	23.5	1 2 0	9.7	12.4	5 2 $\bar{8}$	50.3	41.9
6 0 $\bar{2}$	24.4	23.7	1 1 $\bar{6}$	*	2.0	1 2 1	*	11.3	6 2 $\bar{1}$	*	3.2
6 0 $\bar{4}$	14.9	14.5	1 1 $\bar{7}$	*	4.1	1 2 2	123.9	120.4	6 2 $\bar{2}$	*	11.6
6 0 $\bar{6}$	61.4	61.8	1 1 $\bar{8}$	*	6.5	1 2 3	*	3.9	6 2 $\bar{3}$	*	7.3
6 0 $\bar{8}$	*	1.7	2 1 $\bar{1}$	110.8	112.7	1 2 4	*	17.2	6 2 $\bar{4}$	45.3	48.7
7 0 $\bar{2}$	*	18.9	2 1 $\bar{2}$	*	9.1	1 2 5	*	4.7	6 2 $\bar{5}$	*	2.8
7 0 $\bar{4}$	43.8	40.6	2 1 $\bar{3}$	23.1	22.1	1 2 6	*	17.1	6 2 $\bar{6}$	67.3	40.8
7 0 $\bar{6}$	*	7.5	2 1 $\bar{4}$	57.5	54.5	2 2 0	*	1.4	0 2 1	*	2.6
7 0 $\bar{8}$	*	3.9	2 1 $\bar{5}$	*	5.1	2 2 1	*	10.5	0 2 2	*	8.2
8 0 $\bar{2}$	23.4	27.4	2 1 $\bar{6}$	*	18.7	2 2 2	33.6	8.4	0 2 3	*	11.5
8 0 $\bar{4}$	*	1.8	2 1 $\bar{7}$	18.0	16.6	2 2 3	*	3.8	0 2 4	*	11.5
8 0 $\bar{6}$	*	7.2	2 1 $\bar{8}$	*	2.4	2 2 4	67.3	64.8	0 2 5	*	12.2
8 0 $\bar{8}$	*	6.5	2 1 $\bar{9}$	42.9	44.7	2 2 5	*	3.7	0 2 6	*	2.8
0 1 1	37.4	36.7	3 1 $\bar{1}$	20.6	15.0	2 2 6	*	4.2	0 2 7	*	9.1
0 1 2	*	1.6	3 1 $\bar{2}$	79.8	73.4	3 2 0	19.2	23.3	0 2 8	41.4	40.0
0 1 3	52.4	57.3	3 1 $\bar{3}$	10.3	14.6	3 2 1	*	9.3			
0 1 4	*	1.2	3 1 $\bar{4}$	*	13.0	3 2 2	*	8.5			
0 1 5	54.3	70.7	3 1 $\bar{5}$	13.1	15.2	3 2 3	*	11.6			

\* Denotes an unobserved reflection.

two metal atoms (Table 4), which are consistent with the known crystal chemistry of titanium and vanadium. A difference Fourier map, calculated at the end of the refinement, showed no new structural features but gave peaks around the metal atoms typical of anisotropic thermal motion, resulting from the inadequate absorption correction.

*Description of structure: relationship to rutile and diasporite structures*

The structure of tivanite is viewed along *b* in Figures 2 and 3, which show the closest-packing of the anions and the articulation of the octahedra respectively. The structure represents a new  $M(\text{O},\text{OH})_2$  type based on a two-layer closest-packed oxygen framework with octahedrally coordinated metals distributed equally in the two layers, adding to the well known rutile-type,  $\alpha\text{-PbO}_2$ -type, and diasporite-type structures (and the distorted rutile-type structures such as  $\text{VO}_2$  and  $\text{InOOH}$ ). Actually, the tivanite

structure may be considered as a simple 1:1 intergrowth of rutile- and diasporite-type structures, parallel to  $(0\bar{3}1)_{\text{rutile}}$ . This is shown in Figure 2, where the two structure types are delineated by heavy lines. The intergrowth is on the finest possible scale that still maintains a unit-cell repeating unit of the two contributing structures. As is apparent in Figure 2, this leads to interpenetration of the two structure types. This intergrowth model suggests an assignment of  $\text{Ti}^{4+}$  to site  $M(1)$  and  $\text{V}^{3+}$  to site  $M(2)$ , corresponding to the  $\text{TiO}_2$  (rutile-type) and  $\text{VOOH}$  (diasporite-type) parts of the structure.

Because of the very similar scattering factors, we were unable to establish from the structure refinement whether ordering existed. The mean bond lengths of  $M(1)$ , 2.00(4)Å, and  $M(2)$ , 2.03(4)Å, are not significantly different. The observed ranges for  $M(1)\text{-O}$  and  $M(2)\text{-O}$  are consistent with those observed for  $\text{Ti}^{4+}$  and  $\text{V}^{3+}$  in other closest-packed structures such as derbylite (Moore and Araki, 1976), da-

Table 4. Tivanite: interatomic distances (Å) and angles (°)

$M(1)$ octahedron	Distance	O-M-O angle	$M(2)$ octahedron	Distance	O-M-O angle
$M(1)\text{-O}(1)$	1.87*		$M(2)\text{-O}(2)$	1.84	
$M(1)\text{-O}(4)$	1.96		$M(2)\text{-O}(4)$	1.91	
$M(1)\text{-O}(4)$	2.02		$M(2)\text{-O}(1)$	2.00	
$M(1)\text{-O}(1)$	2.03		$M(2)\text{-O}(2)$	2.02	
$M(1)\text{-O}(3)$	2.05		$M(2)\text{-O}(3)$	2.18	
$M(1)\text{-O}(2)$	2.09		$M(2)\text{-O}(3)$	2.22	
$O(1)\text{-O}(3)$	2.60	82.7	$O(1)\text{-O}(3)$	2.59	75.6
$O(4)\text{-O}(4)$	2.70	85.4	$O(2)\text{-O}(3)$	2.71	80.3
$O(1)\text{-O}(2)$	2.70	85.8	$O(3)\text{-O}(3)$	2.72	76.3
$O(2)\text{-O}(3)$	2.71	81.7	$O(2)\text{-O}(4)$	2.75	88.8
$O(3)\text{-O}(4)$	2.76	87.0	$O(2)\text{-O}(3)$	2.78	81.7
$O(1)\text{-O}(4)$	2.81	89.2	$O(2)\text{-O}(2)$	2.81	93.6
$O(2)\text{-O}(4)$	2.84	88.9	$O(2)\text{-O}(4)$	2.86	99.2
$O(1)\text{-O}(1)$	2.87	94.5	$O(1)\text{-O}(3)$	2.89	87.4
$O(1)\text{-O}(3)$	2.88	89.5	$O(3)\text{-O}(4)$	2.90	88.8
$O(1)\text{-O}(4)$	2.94	92.9	$O(1)\text{-O}(4)$	2.94	97.7
$O(2)\text{-O}(4)$	3.04	95.6	$O(2)\text{-O}(3)$	2.98	95.1
$O(1)\text{-O}(4)$	3.08	104.7	$O(1)\text{-O}(2)$	3.10	107.8
<u>Metal-metal distances</u>					
$M(1)\text{-}M(1)'$	$e^\dagger$	2.92	$M(1)\text{-}M(2)$	$c^\dagger$	3.37
$M(1)\text{-}M(2)$	$e$	3.12	$M(1)\text{-}M(1)'$	$c$	3.48
$M(1)\text{-}M(2)'$	$e$	3.14	$M(1)\text{-}M(2)'$	$c$	3.50
$M(2)\text{-}M(2)'$	$e$	3.47	$M(1)\text{-}M(2)''$	$c$	3.60

\* The standard deviations for distances  $M\text{-}M$ ,  $M\text{-}O$ , and  $O\text{-}O$  are 0.01, 0.04, and 0.06 Å respectively, and the standard deviation for angle  $O\text{-}M\text{-}O$  is 1.5°.

†  $e$  and  $c$  refer to edge- and corner-shared linkages.

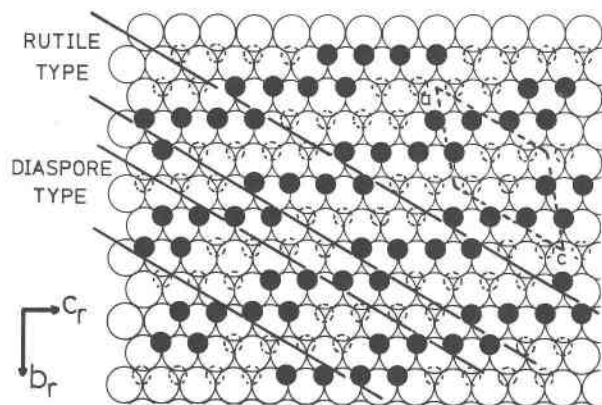


Fig. 2. The structure of tivanite, viewed along  $b_m$ , showing a closest-packed anion layer at  $y = 1/4$  and the metal-atom arrangement at  $y = 1/2$  (filled circles) and  $y = 0$  (dashed circles). The unit-cell outline is shown by dashed lines. The heavy lines parallel to  $c_m$  delineate the rutile-type and diaspore-type elements of the 1:1 intergrowth. The rutile axes  $b_r$  and  $c_r$  are also shown.

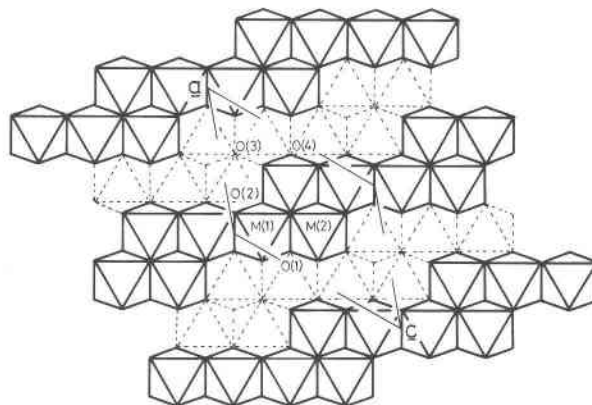


Fig. 3. Polyhedral representation of the tivanite structure, viewed approximately along  $b_m$ . Polyhedra centered at  $y = 1/2$  are outlined with heavy lines. Polyhedra centered at  $y = 0$  are shown by dashed lines.

vidite (Gatehouse *et al.*, 1979), and montroseite (Evans and Block, 1953). The intergrowth model suggests that anion sites O(2) and O(3) in the diaspore part of the structure are the most likely sites for the hydrogen atoms. With  $Ti^{4+}$  in site M(1) and  $V^{3+}$  in site M(2), and with the hydrogen atoms distributed between O(2) and O(3), the latter sites would be oversaturated and the O(1) and O(4) sites would be correspondingly undersaturated by 0.17 valence units. The observed longer bond lengths for M–O(2), O(3) relative to those for M–O(1), O(4) support this model.

Alternatively, the tivanite structure may be considered to derive from the rutile-type structure by the application of the antiphase operation  $\frac{1}{2}[013](0\bar{3}1)$ . Repeated application of this operation to every second  $(0\bar{3}1)$  plane produces the diaspore-type structure. Similarly, repeated application of the antiphase operation  $\frac{1}{2}[0\bar{1}1](011)$ , produces the  $\alpha$ - $PbO_2$ -type structure (Bursill *et al.*, 1971). It is interesting to note that (011), and  $(0\bar{3}1)$ , are both mirror planes for the anion framework (they represent the dominant twin planes in rutile), and that the vectors associated with the above antiphase operations represent the shortest possible displacements in a closest-packed anion framework that leave the anion arrangement invariant.

The diffraction patterns for multiply twinned tivanite are very similar to those for pseudorutile (Grey and Reid, 1975); the diffuse streaks observed in the single-crystal patterns of pseudorutile correspond

closely, in extent and orientation, to the groupings of reflections resulting from the twin variants in tivanite. This suggests that pseudorutile has a microtwinned domain structure based on that of tivanite. The structural relationships between tivanite and pseudorutile are the subject of continuing research in our laboratories.

## References

- Bursill, L. A., Hyde, B. G., and Philp, D. K. (1971) New crystallographic shear families derived from the rutile structure. *Philosophical Magazine*, 23, 1501–1513.
- Evans, H. T., Jr., and Block, S. (1953) The crystal structure of montroseite, a vanadium member of the diaspore group. *American Mineralogist*, 38, 1242–1250.
- Friedel, G. (1964) *Leçons de Cristallographie*. Blanchard, Paris.
- Gatehouse, B. M., Grey, I. E., and Kelly, P. R. (1979) The crystal structure of davidite. *American Mineralogist*, 64, 1010–1017.
- Grey, I. E., and Reid, A. F. (1975) The structure of pseudorutile and its role in the natural alteration of ilmenite. *American Mineralogist*, 60, 898–906.
- Moore, P. B., and Araki, T. (1976) Derbylite,  $Fe_4Ti_3SbO_{13}(OH)$ , a novel close-packed oxide structure. *Neues Jahrbuch für Mineralogie, Abhandlungen*, 126, 292–303.
- Nickel, E. H. (1977) Mineralogy of the "green leader" gold ore at Kalgoorlie, Western Australia. *Proceedings of the Australasian Institute of Mining and Metallurgy*, No. 263, 9–13.
- Nickel, E. H., and Grey, I. E. (1979) Tomichite, a new oxide mineral from Western Australia. *Mineralogical Magazine*, 43, 469–471.
- Stewart, J. M. (1976) The X-RAY system—version of 1976. Computer Science Center, University of Maryland, TR-446.